Methane Activation by Transition-Metal Oxides, MO_x (M = Cr, Mo, W; x = 1, 2, 3)

Xin Xu,[#] Francesco Faglioni, and William A. Goddard, III*

Materials and Process Simulation Center (139-74), California Institute of Technology, Pasadena, California 91225

Received: December 18, 2001; In Final Form: March 25, 2002

Recent experiments on the dehydrogenation−aromatization of methane (DHAM) to form benzene using a MoO_3/HZSM-5 catalyst stimulated us to examine methane activation by the transition-metal oxide molecules, MO_x (M = Cr, Mo, W; x = 1, 2, 3). The present studies use hybrid density functional theory (B3LYP). The reactivity trend is rationalized in terms of changes in the electrophilicity of MO_x, the strength of the M−O π bond, and the bonding properties of MO_x to methyl or hydrogen as M and x are varied. It is found that σ-bond metathesis to the metal hydride product ($H-MO_{x-1}-OCH_3$) occurs preferentially over the high oxidation state form (MO_3) of the heavier metals, as well as all chromium oxides (CrO_x). Instead, oxidative addition of MO_x leading to methyl metal hydride ($H-M(O_x)-CH_3$) is more favorable over the low oxidation state of MO_x (M = Mo, W, x = 2, 1). In particular, it is found that WO_2 can undergo oxidative addition with negligible activation barrier and is predicted to be the most reactive compound of this class toward methane activation. Our finding that MO_2 (M = W, Mo) is the best oxidation state for this class of metal oxides toward methane activation suggests that the MO_3/HZSM-5 catalysts active in the DHAM reaction may be W and Mo oxycarbides (MO_2C_2). The formation of such intermediates may be the reason that the experiments find an induction period before the catalyst is active for the desired reaction.

1. Introduction

The efficient catalytic conversion of methane to petrochemical feedstocks and liquid fuels is a great technical challenge but quite important to society with the potential to revolutionize natural gas utilization. A very promising approach is the dehydrogenation−aromatization of methane (DHAM) to form benzene in the absence of gas-phase oxygen.[1−19] MoO_3/HZSM-5 is generally believed to be the best catalyst for DHAM and has been widely studied. While pure MoO_3 leads to no formation of benzene and HZSM-5 has very limited activity toward methane activation, the combined system MoO_3/HZSM-5 yields conversions as high as 10% with 80% selectivity toward benzene.[1] This catalyst has an induction period and appears to be poisoned by coke formation.[1] There is general agreement that this system forms a bifunctional catalyst with the metal responsible for methane activation to C_2 species and the zeolite responsible for their conversion to benzene.[1,2,8,20] Barry et al.[11] report that this system contains highly dispersed Mo monomers or dimers that are likely to play a role in the catalytic process. It is not clear, however, what is the active phase or what reaction mechanism activates the methane. For instance, Shu et al.[2] report that pure MoO_3 yields CH_4 conversion of 31.6−50% with 2.6−7.7% selectivity toward C_2H_6, while Wong et al.[3] report 0.01% conversion with 49.1% selectivity toward C_2H_6 and 50.9% toward C_2H_4. Upon exposure to CO_2, ref 4 reports that catalytic activity of Mo-based catalysts are quenched, while ref 5 reports an enhancement in activity and ref 6 claims that a CrO_x catalyst can bear large amounts of CO_2. The activity of W-based catalysts are variously reported as no activity by ref 7, low activity by ref 8, and of the highest activity by ref 9. The active phase for methane activation has been suggested to be MO_x (M = Cr,[6] Mo,[15] W[9]) by refs 6, 9, and 15, MoO_xC_y by refs 14, 16, and 18 and Mo_2C by refs 4 and 12. The C−H bond activation mechanism has been proposed as

$$CH_4 \rightarrow CH_3 + H^2$$

$$CH_4 \rightarrow CH_2 + H_2{}^{19}$$

$$CH_4 \rightarrow CH_3{}^{\delta+} - H^{\delta-7}$$

$$CH_4 \rightarrow CH_3{}^{\delta-} - H^{\delta+1}$$

$$CH_4 + H^+ \rightarrow CH_5{}^+ \rightarrow CH_3{}^+ + H_2{}^{19}$$

The broad range of hypotheses concerning this process is largely because studies of mechanisms for reactions over oxide catalysts are complicated by the irregular structure of the active sites, the complex composition of the catalysts, and the differing reaction conditions of the catalytic processes. To gain an understanding of such complex heterogeneous systems, considerable attention has been devoted to studying the more tractable chemistry of gas-phase metal oxides.[20−26]

The gas-phase metal oxides are typically generated in a plasma environment or by laser ablation of metal plus oxygen systems or of solid metal oxides;[20−26] however, for even the simplest gas-phase reactions, there remain many unresolved issues regarding the reaction mechanisms and the energetics for the processes of interest. Because these gas-phase species provide the simplest model of the heterogeneous active sites, such studies can provide valuable insight into the elementary steps of more complex heterogeneous catalytic processes.

* To whom correspondence should be addressed. E-mail: wag@wag.caltech.edu.

[#] On sabbatical leave. Permanent address: State Key Laboratory for Physical Chemistry of Solid Surfaces, Department of Chemistry, Xiamen University, China.

10.1021/jp014572x CCC: $22.00
Published on Web 07/12/2002

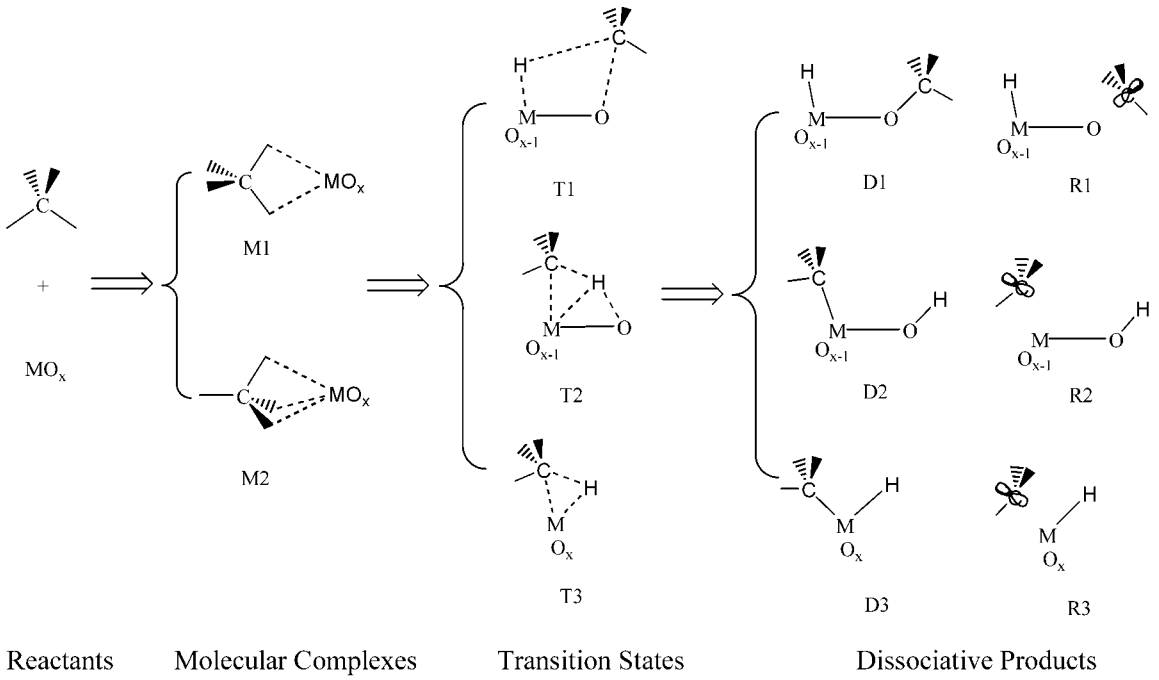

Figure 1. Activation of the methane C−H bond by metal oxide molecules. **M1** and **M2** indicate molecular complexes with methane in pseudo-C_{2v} and -C_{3v} coordinating positions, respectively. **T1** and **T2** are the transition states for two possible σ bond metathesis reactions. **T3** indicates the transition state for the oxidative addition pathway. **D** refers to a dissociative product and **R** to a radical product with the M−CH_3 or O−CH_3 bonds homolytically cleaved. **D1** (H−MO_{x-1}−OCH_3) indicates a hydride product, **D2** (CH_3−MO_{x-1}−OH) a carbide product, and **D3** (H−M(O_x)−CH_3) a methyl metal hydride product. **R1** and **R3** indicate hydride radicals (H−MO_x) and **R2** a hydroxyl radical (MO_x−H).

We present here the first systematic quantum chemical study of methane activation by the transition-metal oxide molecules of MO_x (M = Cr, Mo, W; $x = 1, 2, 3$). This allows us to obtain some of the mechanistic details relevant to the catalytic processes.[27−29] Our purpose is to understand (1) how the C−H is activated, (2) what is the best oxidation state for each of the metals considered, (3) which metal is the most active, and (4) what factors determine the reactivity. We expect that answers to these questions will stimulate new investigations both to validate the mechanistic understanding and to improve catalyst design.

2. Computational Details

All computations were performed using the B3LYP hybrid density functional, which includes a mixture of Hartree−Fock exchange with the Lee−Yang−Parr[30−32] exchange−correlation functional including a generalized gradient approximation. B3LYP method provides good descriptions of reaction profiles, including geometries, heats of reactions, and barrier heights.[33]

We use the Wadt and Hay[34] core-valence (relativistic) effective core potential for the metal center (14 explicit electrons for neutral Cr, Mo, W) with the valence double-ζ contraction of the basis functions (denoted as LACVP** in Jaguar). For O, C, and H, we use the standard 6-31G** basis sets developed by Pople and co-workers.[35−36]

All calculations were carried out with the Jaguar 4.0 program suite.[37] Vibrational frequencies were calculated to ensure that each minimum is a true local minimum (only real frequencies) and that each transition state has only a single imaginary frequency. For each species considered, we investigated all plausible spin states.

3. Results and Discussion

Figure 1 shows the reaction scheme. We optimized two kinds of molecular complexes between CH_4 and MO_x. **M1** corresponds to the pseudo-C_{2v} coordination mode with two methane C−H bonds toward the metal center; while **M2** is in the pseudo-C_{3v} coordination mode with three methane C−H bonds in direct contact with the metal center. **M1** and **M2** can be further classified into the staggered or the eclipsed configurations based on the relative position of C−H bonds and M−O bonds (cf. Table 2 in Supporting Information).

We considered three kinds of transition states: **T1** leading to **D1** (H−MO_{x-1}−OCH_3), **T2** leading to **D2** (CH_3−MO_{x-1}−OH), and **T3** leading to **D3** (H−M(O_x)−CH_3). In the **T1** transition state, methane approaches the M−O bond from the O end with H attacking the metal and the methyl group attacking the oxygen. We refer to the resulting species (**D1**) as the hydride product (it has a M−H bond). In the **T2** transition state, methane approaches MO_x with its methyl group attacking the metal. We refer to the resulting product, **D2**, as the carbide product (it has a M−CH_3 bond). These two processes correspond to [$2_s + 2_s$] additions, often denoted as σ-bond metathesis. The reaction leading to product **D3** is generally referred to as oxidative addition, with the metal center M formally oxidized by two units simultaneous with forming the new M−H and M−CH_3 bonds. **D3** might also be referred to as methyl metal hydride product. As shown in Figure 1, **R1**, **R2**, and **R3** are the radical products formed by homolytic cleavage of the corresponding C−M and C−O bond from **D1**, **D2**, and **D3**.

3.1. MO_x Description. Table 1 summarizes the properties of the electronic ground state of the metal oxides. For MO_3, the ground state is always singlet, corresponding formally to a double bond from the M to each O. Here, the positive charge on the metal center increases from Cr (+1.12) to Mo (+1.44) to W(+1.53).

Because of the increased exchange stabilization of the singly occupied (nonbonding) d orbitals, high spin states become more and more favorable as the metal oxidation state is reduced. However, there are distinct differences, which can be understood

TABLE 1: Electronic Properties of the Ground States of MO_x[a]

	spin states			electronic configurations			Mulliken charges		
	Cr	Mo	W	Cr	Mo	W	Cr	Mo	W
MO	5	5	3	$s^{0.68}p^{0.25}d^{4.59}$	$s^{0.76}p^{0.23}d^{4.53}$	$s^{1.67}p^{0.14}d^{3.80}$	0.47	0.46	0.39
MO_2	3	3	1	$s^{0.18}p^{0.31}d^{4.58}$	$s^{0.37}p^{0.29}d^{4.38}$	$s^{1.18}p^{0.28}d^{3.67}$	0.94	0.96	0.87
MO_3	1	1	1	$s^{0.22}p^{0.28}d^{4.38}$	$s^{0.16}p^{0.29}d^{4.11}$	$s^{025}p^{0.35}d^{3.85}$	1.12	1.44	1.53

[a] WO_x has lower spin multiplicity and higher s orbital occupation than CrO_x and MoO_x for $x = 1$ and 2. This parallels the trend that the atomic configuration of W is s^2d^4 and the atomic configuration of Cr or Mo is s^1d^5. When $x = 3$, charges on the metal centers follow the trend that $WO_3 > MoO_3 > CrO_3$.

TABLE 2: Binding Energies of Molcular Complexes[a]

M	$CH_4\cdots MO_3$	$CH_4\cdots MO_2$	$CH_4\cdots MO$
Cr	13.5	10.6	3.7
Mo	12.6	7.5	1.9
W	15.3	2.1	0.3

[a] All energies (kcal/mol) are referred to the corresponding ground states of $CH_4 + MO_x$. Binding energies become smaller as x goes from 3 to 1 and as M goes down the column from CrO_x to WO_x for $x = 2$, 1. Binding is strongest for WO_3.

TABLE 3: Charge Transfer from CH_4 to MO_x in the Molecular Complex $CH_4\cdots MO_x$

M	$CH_4\cdots MO_3$	$CH_4\cdots MO_2$	$CH_4\cdots MO$
Cr	0.22	0.17	0.15
Mo	0.22	0.19	0.13
W	0.28	0.13	0.03

from the differences in the atomic ground states, which correspond to s^1d^5 for Cr and Mo but s^2d^4 for W. Accordingly, the low oxidation states WO_x ($x = 1$, 2) have lower spin multiplicity and more s character than the respective CrO_x and MoO_x.

For the lower oxidation states, the positive charge on the metal center decreases slightly (<0.09) going from Cr to W. This is in contrast to the trend found for MO_3, where W is more positive than Cr by 0.41. As discussed below, these properties of MO_x are correlated directly to the chemical behavior of these species.

3.2. CH_4-MO_x Molecular Complexes. The interaction between CH_4 and MO_x is attractive when CH_4 approaches MO_x from the metal side. Table 2 summarizes the binding energies. We note the following trends: (1) coordination energies are nearly independent of CH_4 orientation; (2) the stability of the molecular complexes decreases with the oxidation state; (3) for oxidation state VI, the CH_4-MO_3 bond strength is roughly the same for Cr and Mo and only slightly stronger for W; (4) for oxidation states IV and II, the $CH_4-MO_{2,1}$ bond strength decreases from Cr to Mo and to W.

These trends suggest that the attractive interaction of CH_4 and MO_x is electrostatic, involving donation of negative charge from the methane to the metal center. Table 3 reports the changes in Mulliken charges upon formation of the molecular complexes. The binding energy correlates roughly with the amount of charge transferred from methane to metal upon coordination. To form a strong bond for the complex, it is important to have the metal center be electrophilic and to have available vacant frontier orbitals of the correct symmetry (s for C_{3v} coordination and s + d for C_{2v} coordination). For oxidation state VI, W possesses the highest positive charge and forms the strongest bond to CH_4. For oxidation states IV and II, W has the highest s occupation, which pushes away the CH_4 leading to the least stable $CH_4-MO_{2,1}$ molecular complexes.

3.3. Dissociative Products. The relative energy of the various products depends on separately measurable factors such as (1) the promotion energy to bring the metal in a reactive state and the changes in the exchange energy during the reaction, (2) the π binding energy for M−O bonds, and (3) the bond energies for M−H/M−CH_3 and O−H/O−CH_3 bonds. In Table 4, the strength of the M−O π bond in MO_x is estimated by singlet−triplet splitting for the orbitals involved in the π bond. The π bond is weakest in MO_3 because of the spectator oxo effect.[38,39] For lower oxidation states, the π bond strength is larger and roughly constant for a given metal M (except for Cr where the loss of exchange energy upon formation of the π bond is most significant). The π bond becomes stronger for heavier metals, $CrO_x < MoO_x < WO_x$, for each value of x. This is partly because the smaller d−d exchange stabilization for heavier elements leads to a smaller loss for bonding these orbitals.

TABLE 4: Spin Excitation Energies (kcal/mol) for MO_x[a]

	M−O	OM−O	O_2M-O
Cr	25.0	32.3	19.1
Mo	51.0	51.8	36.5
W	68.0	65.0	34.0

[a] These energies can be related to the strengths of the M−O π bonds. The M−O π bond gets stronger as M varies from Cr to W and x varies from 3 to 1.

TABLE 5: Strengths of $X-MO_x$ and $X-OMO_{x-1}$ Bonds (kcal/mol)[a]

	CH_3-MO_x	$H-MO_x$	CH_3-OMO_{x-1}	$H-OMO_{x-1}$
Cr	53.1	53.4	100.0	122.1
Mo	67.9	72.6	101.3	123.0
W	81.0	82.8	102.4	124.5

[a] The values refer to homolytic dissociation of the bond without formation of the M−O π bond in the resulting fragments. The $X-MO_x$ bond becomes stronger as M goes down the column from Cr to W. The $X-OMO_{x-1}$ bond strength depends little on M. $X-MO_x$ and $X-OMO_{x-1}$ bond energies show little dependence on the oxidation state of M. CH_3-MO_x and $H-MO_x$ are of similar strength, while CH_3-OMO_{x-1} bond energy is about 20 kcal/mol weaker than $H-OMO_{x-1}$.

Table 5 lists the strengths for the $R-MO_x$ and $R-OMO_{x-1}$ bonds, where R = CH_3 or H. The results can be generalized as follows: (1) The bond $R-MO_x$ is essentially covalent and similar for all oxidation states of M for a given pair of R and M. The CH_3-OMO_{x-1} and the $H-OMO_{x-1}$ bond strengths are about 100 and 120 kcal/mol, respectively. That is, the $H-OMO_{x-1}$ bond is consistently about 20 kcal/mol stronger than the corresponding CH_3-OMO_{x-1} bond. This is similar to the bond strength of CH_3-OCH_3 (83.2 kcal/mol),[40] which is ~20 kcal/mol smaller than that of $H-OCH_3$(104.2 kcal/mol).[40] (2) The strength of a CH_3-MO_x bond is comparable to that of a $H-MO_x$ bond for a given metal, in analogy to CH_3-H (104.9 kcal/mol)[40] vs H−H (104.2 kcal/mol).[40] (3) The $R-MO_x$ bond becomes stronger as the metal goes down the column.

Table 6 illustrates the reaction energetics for the formations of the hydride **D1** ($H-MO_{x-1}-OCH_3$), the carbide **D2** ($CH_3-MO_{x-1}-OH$), and the methyl metal hydride **D3** ($H-M(O_x)-CH_3$). Negative values indicate exothermic reaction with the product thermodynamically more stable than the reactants. As reported in Table 6, **D1** is unstable for WO and MoO, while

TABLE 6: Relative Energies (kcal/mol) of the Hydride D1 ($H-MO_x-CH_3$), the Carbide D2 (CH_3-MO_x-H), and the Methyl Metal Hydride D3 ($H-CH_3-MO_x$) Products[a]

	$x = 3$	$x = 2$	$x = 1$
	$H-MO_x-CH_3$ **D1** Formation		
Cr	−17.0	−9.2	−15.9
Mo	−21.5	−9.4	0.0
W	−35.7	−7.5[b]	23.0
	CH_3-MO_x-H **D2** Formation		
Cr	−38.5	−27.0	−31.9
Mo	−39.9	−24.0	−14.9
W	−53.9	−22.0	2.8
	$H-CH_3-MO_x$ **D3** Formation		
Cr		10.7[b]	3.9[b]
Mo		−26.8[b]	−22.5[b]
W		−46.4	−27.3[b]

[a] Negative values indicate exothermicity with respect to the corresponding ground states of $CH_4 + MO_x$. Oxidative addition is most feasible over MoO_x and WO_x for $x = 2, 1$. Carbide formation is most feasible over CrO_x ($x = 1-3$), MoO_3, and WO_3. [b] Indicates that the product does not have the same spin multiplicity as the corresponding ground state of MO_x.

D2 is unstable for WO. Oxidative addition (**D3** formation) is always unfavorable for CrO_x. Of course, this oxidative addition does not occur for the high oxidation state of MO_3.

To form the hydride or carbide products from the reactants, it is necessary to break a M−O π bond. Thus, the observation that **D1** or **D2** formation is most exothermic for MO_3 is consistent with these oxides having the weakest π bonds.

Also, the observation that the $R-MO_3$ bond strength increases as the metal changes from Cr to W correlates well with the relative stability of $H-MO_{x-1}-OCH_3$ and $CH_3-MO_{x-1}-OH$. Again, $CH_3-MO_{x-1}-OH$ formation is about 20 kcal/mol more exothermic than $H-MO_{x-1}-OCH_3$ formation, paralleling the trend that the O−H bond is about 20 kcal/mol stronger than the $O-CH_3$ bond.

The interplay between the strengths of a M−O π bond and the $R-MO_x$ bonds is responsible for the computed trends in exothermicity as M changes from Cr to Mo to W. First, CrO_x favors $CH_3-MO_{x-1}-OH$ (**D2**) formation over $H-M(O_x)-CH_3$ (**D3**) formation for all oxidation states because the Cr−O π bond is the weakest and the sum of CH_3-CrO_x and $H-CrO_x$ bond energies is not sufficient to compensate for the energy cost of breaking the methane C−H bond. Then, as the oxidation state decreases, the M−O π bond strength changes (Table 4) and the exothermicity of **D2** formation changes accordingly. Furthermore, in the case of Mo and W, the CH_3-M and H−M bonds are strong enough to favor **D3** over **D2** whenever formation of **D3** is possible. Oxidative addition to form the methyl metal hydride generally leads to a low spin state (the metal center is formally oxidized by two units), while a high spin state is more stable for the low oxidation states of MO_x ($x = 2,1$). Accordingly, the spin multiplicity changes during the oxidative addition.

3.4. Radical Products. Table 7 summarizes the relative energies of the hydride radicals **R1** and **R3** ($H-MO_x$) and the hydroxyl radical **R2** (MO_x-H). Breaking the $M-CH_3$ or the $O-CH_3$ bond to form the radical products is less favorable than dissociative product formation. The general trends are as follows: (1) All reactions to form radical products are endothermic. (2) When the $H-MO_x$ bond is stronger, the hydride radical formation is less endothermic. This leads to the observation that the stability of $H-MO_x$ increases as M goes down the column and x changes from 3 to 1. (3) Because the hydride bond is fairly independent from the oxidation state, the stability of the hydroxyl radical MO_x-H is determined by the strength of the M−O π bond. Accordingly, **R2** formation is most favorable over CrO_x ($x = 3, 2, 1$) or MO_3 (M = Cr, Mo, W).

TABLE 7: Relative Energies (kcal/mol) of the Hydride Radicals R1 and R3 ($H-MO_x$) and the Hydroxyl Radicals R2 (MO_x-H)[a]

	$x = 3$	$x = 2$	$x = 1$
	$H-MO_x$ **R1** and **R3** Formation		
Cr	81.8	64.1	54.6
Mo	79.0	46.7	43.5
W	65.8	32.3	30.1
	MO_x-H **R2** Formation		
Cr	13.6	23.8	17.6
Mo	29.6	44.3	42.1
W	25.6	55.0	56.6

[a] Positive values indicate endothermicity with respect to the corresponding ground states of $CH_4 + MO_x$. Radical mechanisms are less plausible. CrO_x is the best candidate for a radical mechanism to happen.

TABLE 8: Activation Energies (kcal/mol) for σ Bond Metathesis (T1 and T2) and Oxidative Addition (T3) of MO_x[a]

	$x = 3$	$x = 2$	$x = 1$
	T1 Mechanism		
Cr	40.5	52.0	56.0
Mo	43.7	58.6	54.5
W	32.2	63.1[b]	70.6[b]
	T2 Mechanism		
Cr	7.7	10.0	10.0
Mo	12.3	23.5	32.9
W	4.0	32.0[b]	58.7
	T3 Formation		
Cr		19.1[b]	25.4[b]
Mo		3.9[b]	7.6[b]
W		−0.4	18.7

[a] All energies are relative to the corresponding ground states of $CH_4 + MO_x$. [b] Indicates change of spin multiplicity during the reaction.

3.5. Transition States. Table 8 lists the activation energies corresponding to transition states **T1**, **T2**, and **T3** in Figure 1. The general trend can be rationalized in terms of both electrostatic and orbital interactions, see Figure 2.

With the exception of **T3** on Cr, the activation barriers follow the trend **T1** > **T2** > **T3**. The relative heights of **T1** and **T2** appear to arise mainly from electrostatic factors (Figure 2a). In **T1**, the interaction between the dipoles associated with the C−H and M−O bonds tends to raise the energy. To contrast this effect, the C−H bond polarizes toward the product charge distribution, forming a negatively charged hydrogen. In **T2**, the electrostatic interaction lowers the energy and no further rearrangement of charges occurs. Thus, it is reasonable that **T2** has a lower energy than **T1**.

In the nucleophilic attack of CH_4 on MO_x (**T2**), the reaction is concerted with a four-center, four-electron cyclic transition state, see Figure 2b. Consistent with this, the activation barriers for **T2** depend strongly on the strength of the M−O π bond. The general trends of the reactivity of MO_x via **T2** are CrO_x > MoO_x > WO_x and MO_3 > MO_2 > MO. The abnormal behavior of the reactivity of MO_3 in **T2** can be explained by considering the relative size of s and d orbitals. The d orbitals are compact for the first-row transition metal; while the d and the s orbitals are comparable in size for the third-row transition metal. The large size of d orbitals in W makes WO_3 react more easily than does CrO_3, even though the W−O π bond is stronger than the Cr−O π bond.

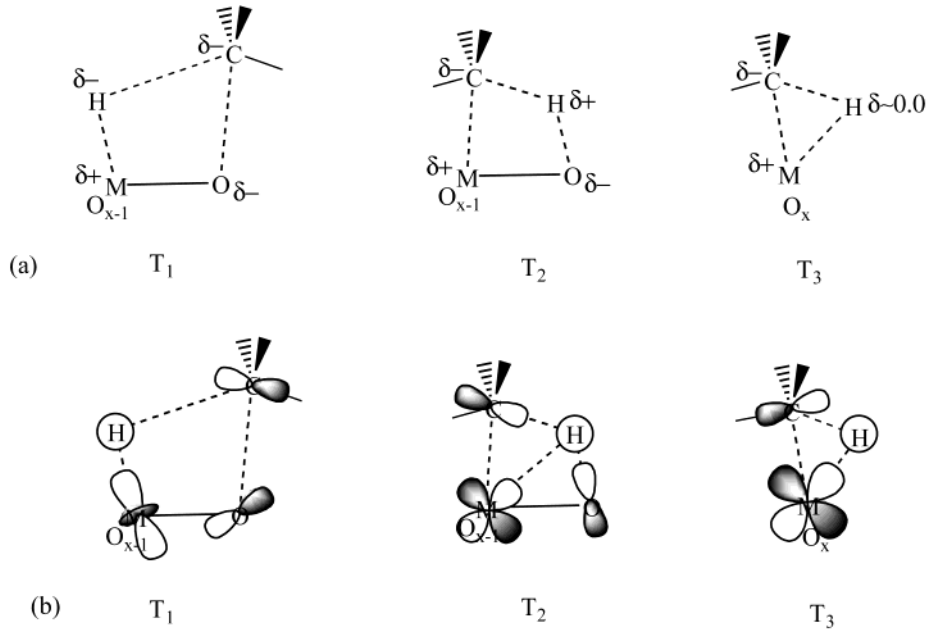

Figure 2. Electrostatic interactions (a) and orbital interactions (b) in the transition states of **T1**, **T2**, and **T3**. The electrostatic interactions in **T1** are not as favorable as those in **T2**, resulting in higher activation energies. Both **T1** and **T2** involve breaking of the M−O π bond making **T3** lower in energy (with exceptions described in the text).

T3 is concerted with a cyclic three-center, four-electron transition state. The activation barrier for **T3** is generally small because it does not require breaking the M−O π bond. The reactivity follows the trend $WO_x > MoO_x > CrO_x$ ($x = 2,1$), as expected from the relative size of the d orbitals, with the exception of WO. For WO, the reactant ground state contains a doubly occupied s orbital (recall that the ground state of W is s^2d^4) on the metal, which prevents the methane from attaining a good transition-state geometry, leading to higher activation energy. The deciding factor for the high activation barrier of CrO_x is the unfavorably compact d orbital. We note that CH_4 can undergo the oxidative addition on WO_2 with practically no activation barrier. In fact, even though the transition state **T3** is above the energy of the molecular complex, it is below the energy level of $CH_4 + WO_2$. Except for WO_x, forming **T3** requires a decrease in spin multiplicity. Thus, the barrier should correlate with the spin excitation energy, which is 19.4 (Cr) and 13.7 (Mo) kcal/mol from the ground-state triplet to the singlet of MO_2 and 22.7 (Cr) and 10.8 (Mo) kcal/mol from the ground-state quintet to the triplet of MO.

Note that the data in Tables 6 and 8 indicate that the optimum spin state sometimes changes during a reaction. For strong spin−orbit coupling (e.g., W), such reactions can be allowed during the time scale of a reaction. However, for weak coupling (e.g., Cr), the actual processes may be spin-allowed (involving either an excited spin state of the reactant or of the product). Further discussion of such surface crossings is found in refs 26−29 and 41.

3.6. Discussion of DHAM Catalysis. On the basis of these findings for simple gas-phase molecules, we speculate that for the more complicated catalysts observed to activate CH_4 to form ethylene and benzene, the reactions will involve mechanism **T2** or **T3** or both, depending on the metal and the oxidation conditions. Although the presence of a heterogeneous support and of additional elements may affect the chemistry of the active centers, our results demonstrate that methane activation can occur with low activation barriers over metal oxides.

We expect that carbide formation is favored by high oxidation states, as well as by high positive charge and low s-orbital population on the metal center. To undergo oxidative addition requires that the metal center is in an intermediate or low oxidation state. Our finding that MO_2 (M = W, Mo) is the best oxidation state for this class of metal oxides toward methane activation suggests that the MO_3/HZSM-5 catalysts active in the DHAM reaction may be W and Mo oxycarbides (MO_2C_2). The formation of such intermediates may be the reason that the experiments find an induction period before the catalyst is active for the desired reaction.

4. Conclusions

We examined the activation of methane by transition-metal oxide molecules of the form MO_x (M = Cr, Mo, W; $x = 1$, 2, 3) using hybrid density functional theory (B3LYP). We find that the trends in reactivity can be rationalized in terms of the electrophilicity of the MO_x, the strength of M−O π bonds, and the binding energies of the MO_x to methyl and hydrogen.

The main results can be summarized as follows:

(1) The molecular complex CH_4−MO_x is stable. The binding between CH_4 and MO_x is dominated by charge-induced dipole-moment interaction. The trends in the relative stability of CH_4−MO_x are

$$MO_3 > MO_2 > MO; \quad CrO_x < MoO_x < WO_x \quad \text{for} \quad x = 3$$
$$\text{and} \quad CrO_x > MoO_x > WO_x \text{ for } x = 2, 1$$

paralleling the trends in the electrophilicity of MO.

(2) As the oxidation state decreases, the M−O π bond strength increases, leading to the π bond strengths in the order $MO > MO_2 > MO_3$ for a given M. The π bond becomes stronger according to the trend $CrO_x < MoO_x < WO_x$ for a given x.

(3) The bond R−MO_x (R = H, CH_3) is essentially covalent. Its strength remains constant for a given pair of R and M against varying x. The R−MO_x bond becomes stronger as M changes from Cr to Mo to W. While the strength of the H−MO_x bond is comparable to that of the CH_3−MO_x, the H−OMO_{x-1} bond is about 20 kcal/mol stronger than the CH_3−OMO_{x-1} bond. This

TABLE 9: Feasibility of the Carbide (D2) Formation and the Oxidative Addition (D3) over MO_x

	$x = 3$	$x = 2$	$x = 1$
	CH_3-MO_x-H **D2** Formation		
Cr	excellent	good	good
Mo	good	possible	possible
W	excellent	possible	endothermic
	$H-CH_3-MO_x$ **D3** Formation		
Cr	impossible	endothermic	endothermic
Mo	impossible	excellent	excellent
W	impossible	best	good

leads to a carbide product ($CH_3-MO_{x-1}-OH$) that is about 20 kcal/mol more stable than the hydride product ($H-MO_{x-1}-OCH_3$).

(4) The activation barriers generally follow the trend **T1** > **T2** > **T3**. The σ bond metathesis to produce the hydride product ($H-MO_{x-1}-OCH_3$) is the most favorable reaction for the high oxidation state of MO_3 and for the chromium oxides of CrO_x. Oxidative addition of MO_x, leading to methyl metal hydride ($H-M(O_x)-CH_3$), is the most favorable reaction for the low oxidation states of MO_x (M = Mo, W, x = 2,1). WO_2 can undergo oxidative addition with practically no activation energy and is predicted to be the most reactive species toward methane activation among the MO_x, see Table 9.

Acknowledgment. This work was partially supported by Chevron Corporation. The facilities of the MSC are also supported by grants from DOE-ASCI-ASAP, DOE-FE, ARO-MURI, NSF-MRI, NSF-CHE, NSF-CTE, 3M, Seiko-Epson, General Motors, Avery-Dennison, Kellogg's, Asahi Kasei, Nippon Steel, and the Beckman Institute.

Supporting Information Available: Tables providing comparison between Mulliken and ESP charges, geometries and binding energies of molecular complexes, changes of Mulliken charges upon CH_4 and MO_x interactions, and strengths of $X-MO_x$ and $X-OMO_{x-1}$ bonds. This material is available free of charge via the Internet at http://pubs.acs.org.

References and Notes

(1) Xu, Y.; Lin, L. *Appl. Catal.* **1999**, *A188*, 53.
(2) Shu, J.; Adnot, A.; Grandjean, P. A. *Ind. Eng. Chem. Res.* **1999**, *38*, 3860.
(3) Wong, S. T.; Xu, Y.; Liu, W.; Wang, L.; Guo, X. *Appl. Catal.* **1996**, *A136*, 7.
(4) Wang, D.; Lunsford, J. K.; Rosynek, M. P. *J. Catal*. **1997**, *169*, 347.
(5) Ohnishi, R.; Liu, S.; Dong, Q.; Wang, L.; Ichikawa, M.; *J. Catal*. **1999**, *182*, 92.
(6) Zhang, H.; Kou, Y. *Chem. Commun*. **1999**, 1729.
(7) Wong, S. T.; Xu, Y.; Wang, L.; Liu, S.; Li, G.; Xie, M.; Guo X. *Catal. Lett.* **1996**, *38*, 39.
(8) Weckhuysen, B. M.; Wang, D.; Roysynek, M. P.; Lunsford, J. H. *J. Catal*. **1998**, *175*, 338.
(9) Zeng, J. L.; Xiong, Z. T.; Zhang, H. B.; Lin, G. D.; Tsai, K. R. *Catal. Lett.* **1998**, *53*, 119.
(10) Liu, S.; Wang, L.; Ohnishi, R.; Ichikawa, M. *J. Catal*. **1999**, *181*, 175.
(11) Borry, R. W.; Kim, Y. H.; Huffsmith, A.; Reimer, J. A.; Iglesia, E. *J. Phys. Chem. B* **1999**, *103*, 5787.
(12) Weckhuysen, B. M.; Wang, D.; Roysynek, M. P.; Lunsford, J. H. *J. Catal*. **1998**, *175*, 347.
(13) Meriaudeau, P.; Thu, V. T.; Tiep, L. V. *Catal. Lett.* **2000**, *64*, 49.
(14) Yuan, S.; Li, J.; Hao, Z.; Feng, Z.; Xin, Q.; Ying, P.; Li, C. *Catal. Lett.* **1999**, *63*, 73.
(15) Solymosi, F.; Erdohelyi, A.; Szoke, A. *Catal. Lett.* **1995**, *32*, 43.
(16) Solymosi, F.; Szoke, A.; Cserenyi, J. *Catal. Lett.* **1996**, *39*, 157.
(17) Szoke, A.; Solymosi, F. *Appl. Catal.* **1996**, *142*, 361.
(18) Zhang, J. Z.; Long, M. A.; Howe, R. F. *Catal. Today* **1998**, *44*, 293.
(19) Zhou, T. J.; Liu, A. M.; Mo, Y. R.; Zhang, H. B. *J. Phys. Chem. A* **2000**, *104*, 5787.
(20) Kaldor, A. J.; Cox, D. M.; Zakin, M. R. *Adv. Chem. Phys.* **1998**, *70*, 221.
(21) Sievers, M. R.; Armentrout, P. B. *J. Phys. Chem. A* **1998**, *102*, 10754.
(22) Kretzschmar, I.; Fiedler, A.; Harvery, J. N.; Schroder, D.; Schwarz, H. *J. Phys. Chem. A* **1997**, *101*, 6252.
(23) Sievers, M. R.; Chen, Y. M.; Armentrout, P. B. *J. Chem. Phys.* **1996**, *105*, 6322.
(24) Bare, W. D.; Souter, P. F.; Andrews, L. *J. Phys. Chem. A* **1998**, *102*, 8279.
(25) Fialko, E. F.; Kikhtenko, A. V.; Goncharov, V. B.; Zamaraev, K. I. *J. Phys. Chem. A* **1997**, *101*, 8607.
(26) Schroder, D.; Schwarz, H. *Angew. Chem., Int. Ed. Engl*. **1995**, *34*, 1973.
(27) Tsipis, A. C.; Tsipis, C. A. *J. Phys. Chem. A* **2000**, *104*, 859.
(28) Perry, J. K.; Ohanessian, G.; Goddard, W. A. *Organometallics* **1994**, *13*, 1870.
(29) Yoshizawa, K.; Shiota, Y.; Yamabe, T. *J. Am. Chem. Soc.* **1998**, *120*, 564.
(30) Becke, A. D. *J. Chem. Phys.* **1993**, *98*, 5648.
(31) Lee, C.; Yang, W.; Par, R. G. *Phys. Rev.* **1988**, *B37*, 785.
(32) Vosco, S. H.; Wilk, L.; Nusiair, M. *Can. J. Phys.* **1980**, *58*, 1200.
(33) Baker, J.; Muir, M.; Andzelm, J.; Scheiner, A. In *Chemical Applications of Density-Functional Theory*; Laird, B. B., Ross, R. B., Ziegler, T., Eds.; ACS Symposium Series 629; American Chemical Society: Washington, DC, 1996.
(34) Hay, P. J.; Wadt, W. R. *J. Chem. Phys.* **1985**, *82*, 299. Goddard, W. A., III *Phys. Rev.* **1968**, *174*, 659. Melius, C. F.; Olafson, B. O.; Goddard, W. A., III *Chem. Phys. Lett.* **1974**, *28*, 457.
(35) Hariharan, P. C.; Pople, J. A. *Chem. Phys. Lett.* **1972**, *16*, 217.
(36) Francl, M. M.; Pietro, W. J.; Hehre, W. J.; Binkley, J. S.; Gordon, M. S.; DeFrees, D. J.; Pople, J. A. *J. Chem. Phys.* **1982**, *77*, 3654.
(37) *Jaguar 4.0*; Schrodinger, Inc.: Portland, OR, 2001. *Jaguar 3.5*; Schrödinger, Inc., Portland, OR, 1998. Greeley, B. H.; Russo, T. V.; Mainz, D. T.; Friesner, R. A.; Langlois, J−M.; Goddard, W. A., III; Donnelly, R. E.; Ringnalda, M. N. *J. Chem. Phys.* **1994**, *101*, 4028.
(38) Rappé, A. K.; Goddard, W. A., III *Nature* **1980**, *285*, 311.
(39) Rappé, A. K.; Goddard, W. A., III *J. Am. Chem. Soc.* **1980**, *102*, 5114.
(40) Lide, D. R. *Handbook of Chemistry and Physics*, 74th ed.; CRC Press: Boca Raton, FL, 1993−1994.
(41) Yoshizawa, K.; Shiot, Y.; Yamabe, T. *J. Chem. Phys.* **1999**, *111*, 538.